Supplement of Geosci. Model Dev., 18, 1103–1118, 2025
https://doi.org/10.5194/gmd-18-1103-2025-supplement

Geoscientific Model Development
Open Access
EGU

Supplement of

Sensitivity of predicted ultrafine particle size distributions in Europe to different nucleation rate parameterizations using PMCAMx-UF v2.2

David Patoulias et al.

Correspondence to: Spyros N. Pandis (spyros@chemeng.upatras.gr)

Table S1. Vertical height for each simulated layer.

Layer number	Bottom height (m)	Top height (m)
1	0	60
2	60	150
3	150	260
4	260	400
5	400	590
6	590	820
7	820	1100
8	1100	1670
9	1670	2300
10	2300	2950
11	2950	3650
12	3650	4900
13	4900	6200
14	6200	7500

Table S2. Description of atmospheric measurement sites in Europe used in this work.

Station	Name	Country	Longitude	Latitude
ANB	Annaberg-Buchholz	Germany	50.5717	12.9989
ASP	Aspvreten	Sweden	58.8000	17.3833
BRK	Birkenes II	Norway	58.3885	8.2520
CBW	Cabauw Zijdeweg	Netherlands	51.9703	4.9264
DSN	Dresden-Nord	Germany	51.0650	13.7414
DSW	Dresden-Winckelmannstrasse	Germany	51.0361	13.7306
FNK	Finokalia	Greece	35.3167	25.6667
GDN	Giordan Lighthouse	Malta	36.0722	14.2184
HOH	Hohenpeissenberg	Germany	47.8015	11.0096
HYY	Hyytiala	Finland	61.8500	24.2833
ISP	Ispra	Italy	45.8000	8.6333
KPU	K-puszta	Hungary	46.9667	19.5833
KST	Kosetice (NOAK)	Czech Republic	49.5734	15.0803
MLP	Melpitz	Germany	51.5301	12.9339
MNT	Montseny	Spain	41.7667	2.3500
PRG	Prague-Suchdol	Czech Republic	50.1264	14.3846
USM	Usti n.L.-mesto	Czech Republic	50.6611	14.0403
VAV	Vavihill	Sweden	56.0167	13.1500
VRR	Varrio	Finland	67.7667	29.5833
VSM	TMNT09 Vielsalm	Belgium	50.3040	6.0013
WLD	Waldhof	Germany	52.8022	10.7594
ZUG	Zugspitze-Schneefernerhaus	Germany	47.4165	10.9796
NEO	Costa Navarino	Greece	36.9932	21.6572
PAT	Patra-ICE-HT	Greece	38.2980	21.8092
SPC	San Pietro Capofiume	Italy	44.6553	11.6236
THE	Thessaloniki	Greece	40.6166	23.0333

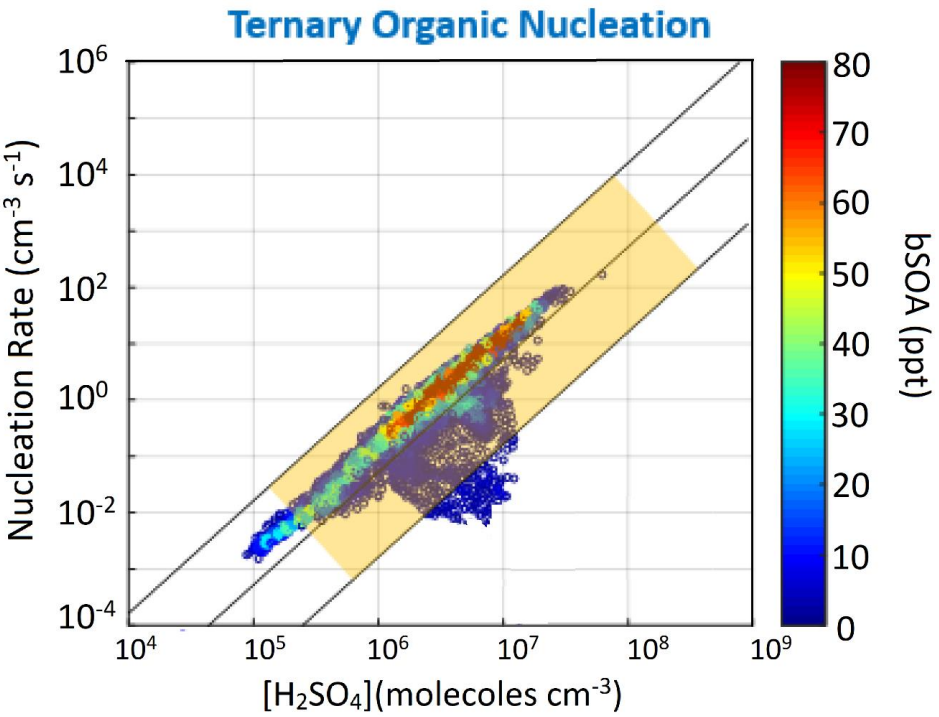

Figure S1. Modeled nucleation rate as a function of H_2SO_4 concentration. Solid diagonal lines provide the bounds for the observations according to Chen et al. (2012).

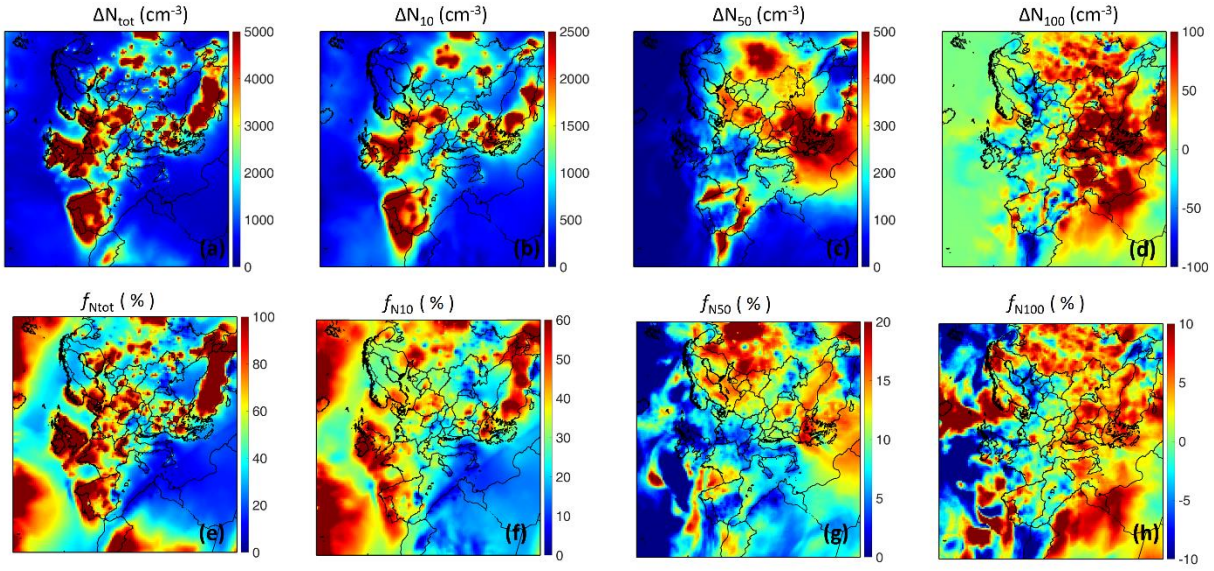

Figure S2. Average ground increase of number concentration (in cm^{-3}) (a-b-c-d) and fractional increase (f_{Nx}) of number concentration (in %) (e-f-g-h) for Case 2 (increase in the nucleation rate by a factor of 10) for ternary ammonia nucleation during 5 June – 8 July 2012 for: (a, e) all particles (f_{Ntot}); (b, f) particles above 10 nm (f_{N10}); (c, g) above 50 nm (f_{N50}); and (d, h) above 100 nm (f_{N100}). Different scales are used.

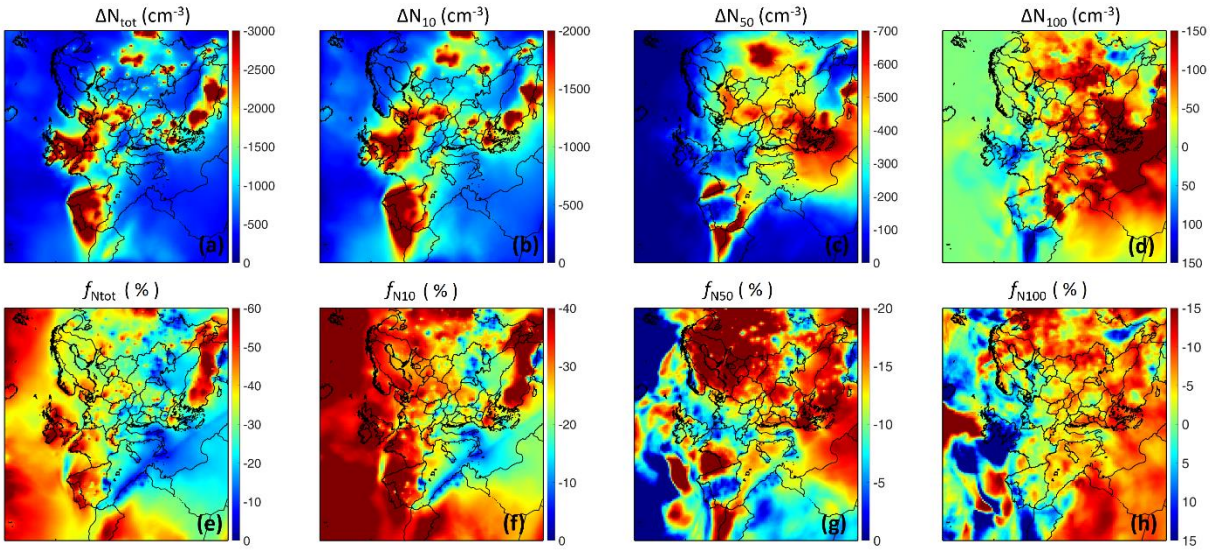

Figure S3. Average ground increase of number concentration (in cm^{-3}) (a-b-c-d) and fractional increase (f_{Nx}) of number concentration (in %) (e-f-g-h) for Case 3 (decrease in the nucleation rate by a factor of 10) for ternary ammonia nucleation during 5 June – 8 July 2012 for: (a, e) all particles (f_{Ntot}); (b, f) particles above 10 nm (f_{N10}); (c, g) above 50 nm (f_{N50}); and (d, h) above 100 nm (f_{N100}). Different scales are used.

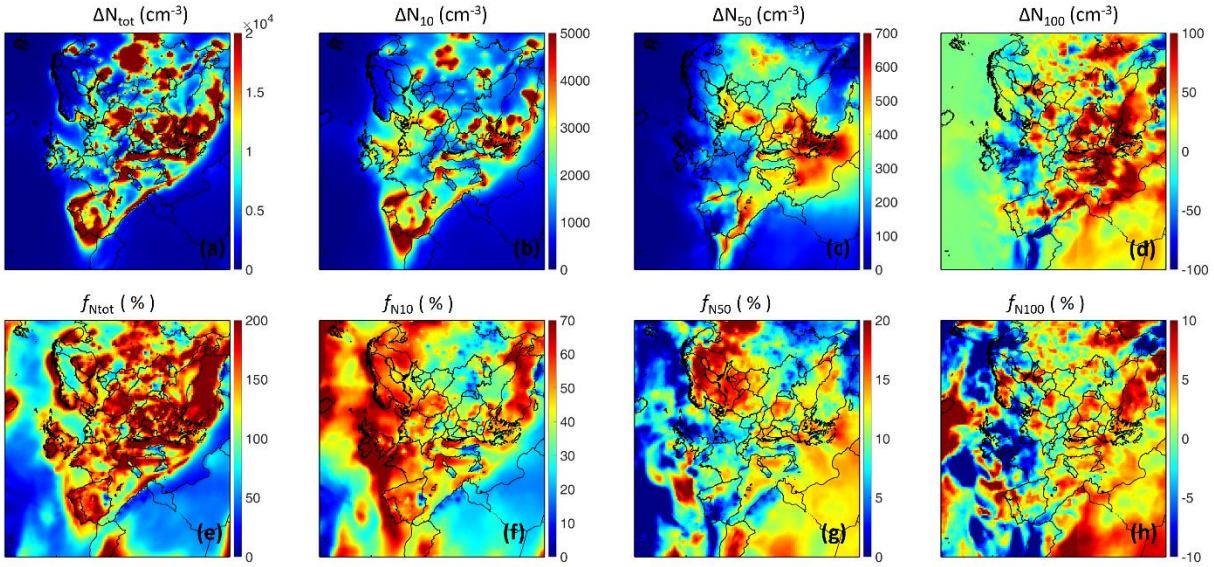

Figure S4. Average ground increase of number concentration (in cm^{-3}) (a-b-c-d) and fractional increase (f_{Nx}) of number concentration (in %) (e-f-g-h) for Case 5 (increase in the nucleation rate by a factor of 10) of organic nucleation during 5 June – 8 July 2012 for: (a, e) all particles (f_{Ntot}); (b, f) particles above 10 nm (f_{N10}); (c, g) above 50 nm (f_{N50}); and (d, h) above 100 nm (f_{N100}). Different scales are used.

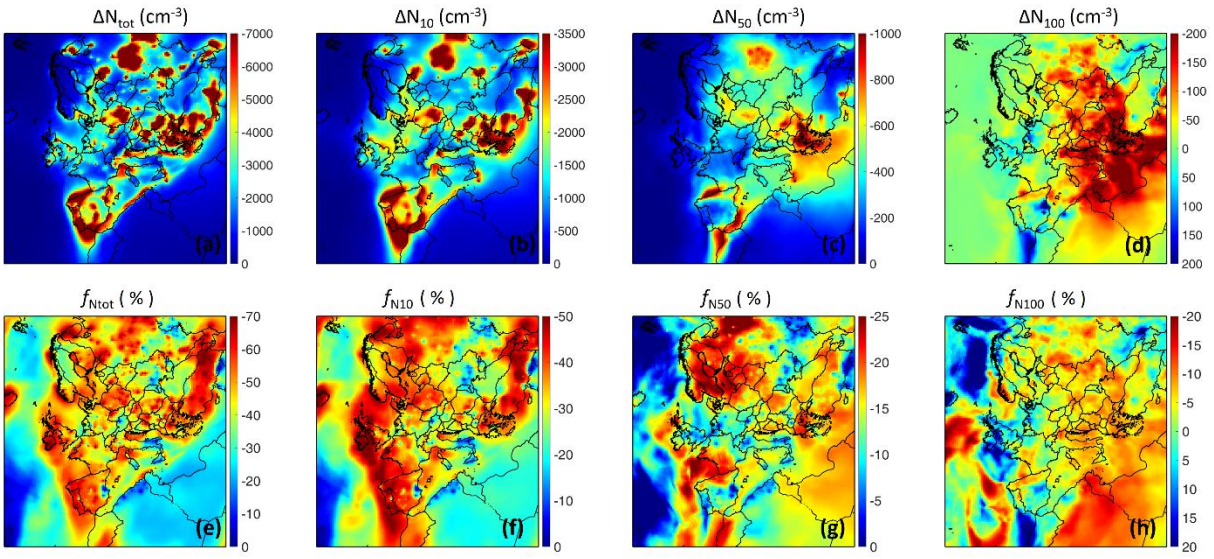

Figure S5. Average ground increase of number concentration (in cm^{-3}) (a-b-c-d) and fractional increase (f_{Nx}) of number concentration (e-f-g-h) for Case 6 (decrease in the nucleation rate by a factor of 10) of organic nucleation during 5 June – 8 July 2012 for: (a, e) all particles (f_{Ntot}); (b, f) particles above 10 nm (f_{N10}); (c, g) above 50 nm (f_{N50}); and (d, h) above 100 nm (f_{N100}). Different scales are used.

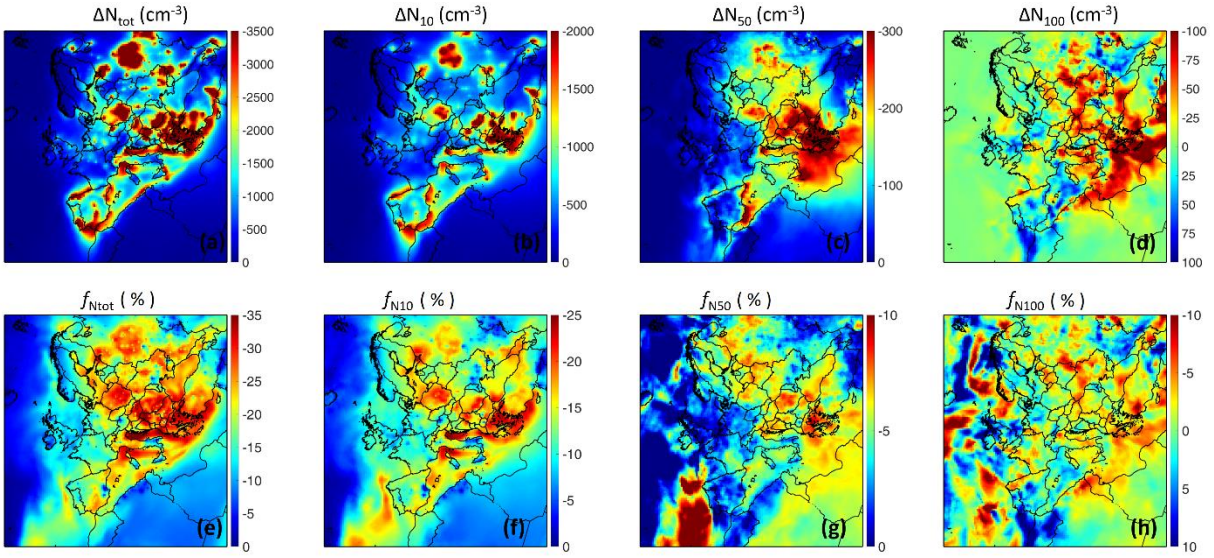

Figure S6. Average ground increase of number concentration (in cm^{-3}) (a-b-c-d) and fractional increase (f_{Nx}) of number concentration (in %) (e-f-g-h) for Case 7 (decrease of nuclei diameter to 1 nm) of organic nucleation during 5 June – 8 July 2012 for: (a, e) all particles (f_{Ntot}); (b, f) particles above 10 nm (f_{N10}); (c, g) above 50 nm (f_{N50}); and (d, h) above 100 nm (f_{N100}). Different scales are used.

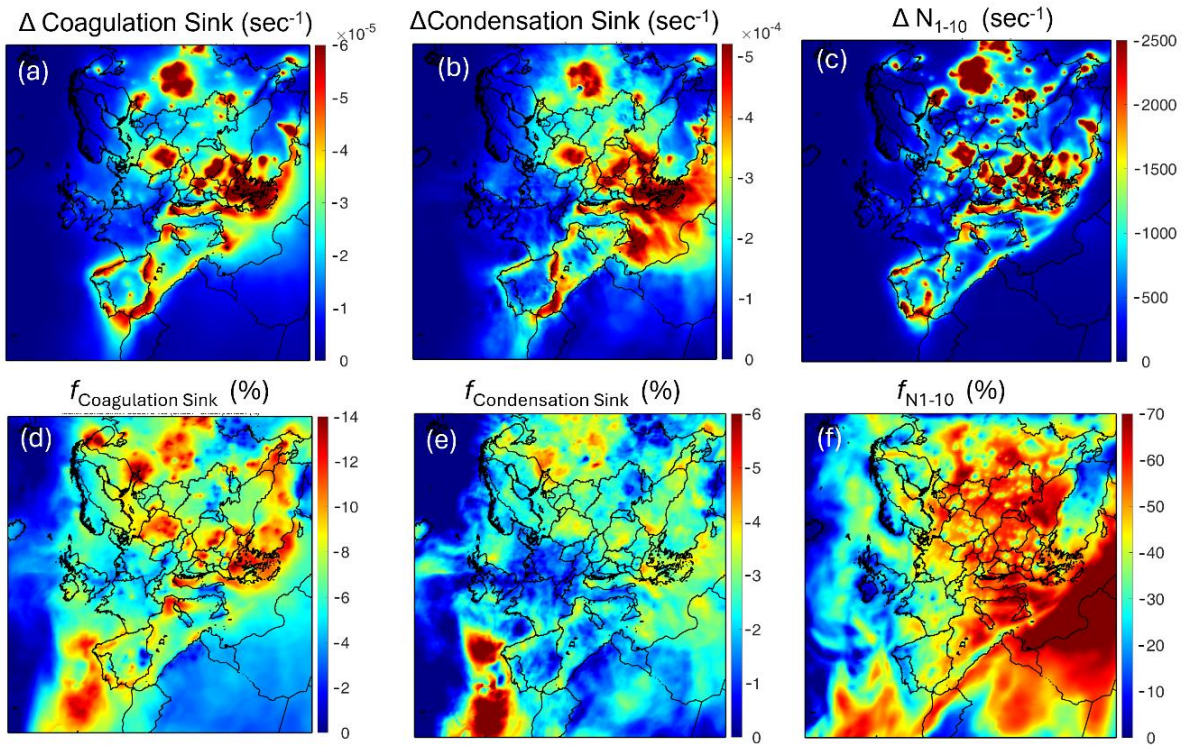

Figure S7. Average ground increase for (a) coagulation sink (in sec^{-1}), (b) condensation sink (in sec^{-1}), (c) number concentration particles between 0.8 nm and 10 nm ($N_{1\text{-}10}$) (in cm^{-3}) and fractional increase (f_{Nx}) of (d) coagulation sink (in %), (e) condensation sink (in %), (f) number concentration particles between 0.8 nm and 10 nm ($N_{1\text{-}10}$) (in %) for Case 7 (decrease of nuclei diameter to 1 nm) of organic nucleation during 5 June – 8 July 2012. Different scales are used.

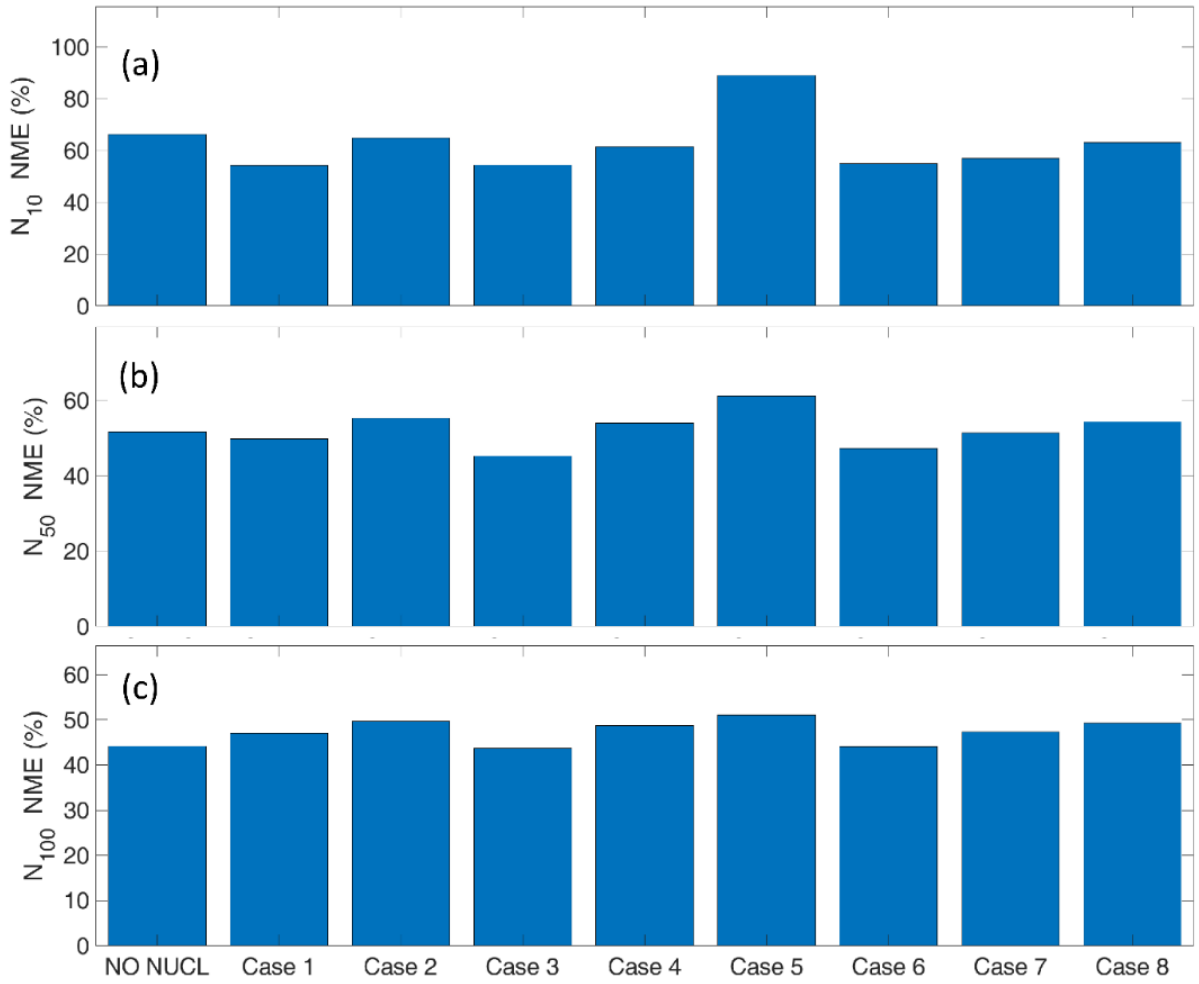

Figure S8. The NME for hourly a) N_{10}, b) N_{50} and c) N_{100} for the no-nucleation scenario, the ammonia ternary parameterization (Case 1) and the change by an order of magnitude in scaling factor (Cases 2 and 3), the biogenic parameterization (Case 4) with the change by an order of magnitude in scaling factor (Cases 5 and 6), decrease of nuclei diameter (Case 7) and the ELVOCs addition as the third species (Case 8).

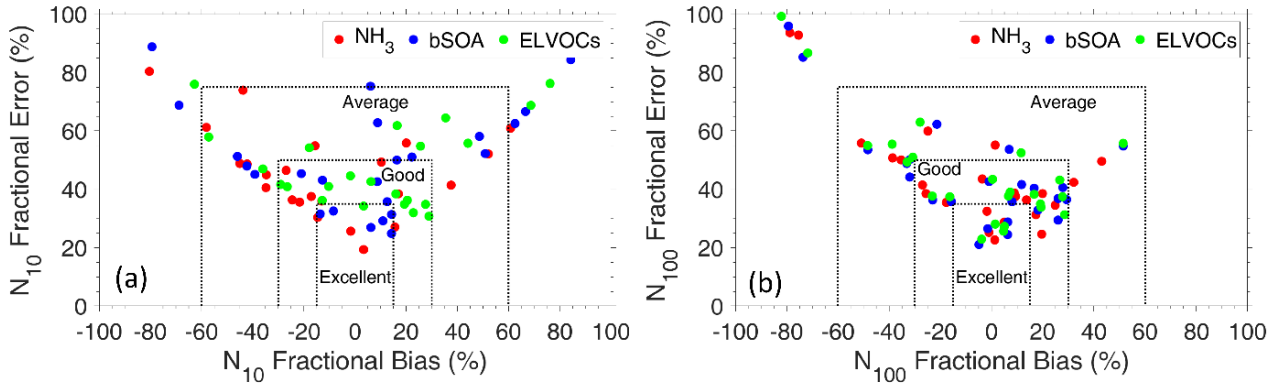

Figure S9. Model evaluation using fractional error (%) versus fractional bias (%) of daily number concentrations for (a) N_{10}, and (b) N_{100} for the ammonia ternary parameterization (Case 1; red dots), the biogenic parameterization (Case 4; blue dots), and the ELVOCs addition as the third species (Case 8).

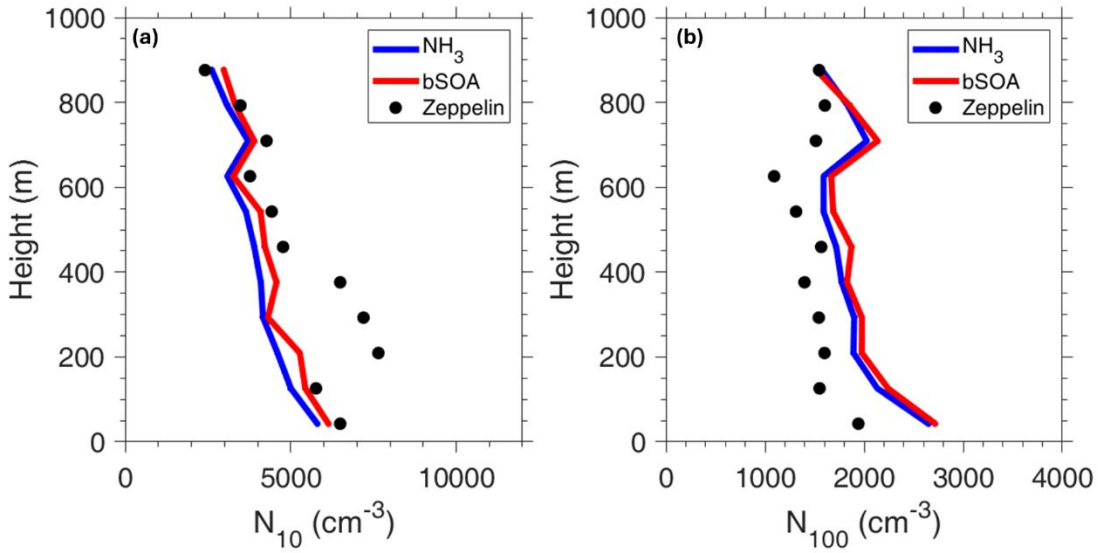

Figure S10. Comparison of predicted PMCAMx-UF for ammonia (blue line) and biogenic SOA (red line) parameterization vs. observed (black dots) vertical profiles of averaged particle number concentrations for (a) N_{10} and (b) N_{100} of 25 flights over the Po Valley during the PEGASOS campaign.